Monthly Notices of the ROYAL ASTRONOMICAL SOCIETY
MNRAS 0, 1–0 (2020) doi:10.1093/mnras/staa2000

Experimental stark widths and shifts of V II spectral lines

J. Manrique,[1] D. M. Díaz Pace,[2] C. Aragón[3,4] and J. A. Aguilera[3,4]★

[1]Facultad de Farmacia, Universidad CEU San Pablo, Urbanización Montepríncipe, Boadilla del Monte, E-28668 Madrid, Spain
[2]Centro de Investigaciones en Física e Ingeniería del Centro de la Provincia de Buenos Aires (CIFICEN), CONICET, CICPBA, Facultad de Ciencias Exactas UNCPBA, Campus Universitario, B7000GHG Tandil, Buenos Aires, Argentina
[3]Departamento de Ciencias, Universidad Pública de Navarra, Campus de Arrosadía, E-31006 Pamplona, Spain
[4]Institute for Advanced Materials and Mathematics (INAMAT2), Public University of Navarre, Campus de Arrosadía, E-31006 Pamplona, Spain

Accepted 2020 July 3. Received 2020 July 3; in original form 2020 June 29

ABSTRACT

We have measured the Stark widths and shifts of V II spectral lines in the wavelength range 2000–4200 Å belonging to 75 multiplets. The spectra are emitted by laser-induced plasmas generated from fused glass discs prepared by borate fusion. The electron density and temperature are in the ranges (0.72–6.5) × 10^{17} cm^{-3} and (11 000–14 900) K, respectively. To avoid self-absorption, we have used seven samples with vanadium concentrations selected by the CSigma graph methodology. This has allowed to include strong and weak lines in the study, including resonance and forbidden lines. The experimental widths and shifts are compared with theoretical values available in the literature.

Key words: atomic data – line: profiles – plasmas.

1 INTRODUCTION

The knowledge of the broadening and shift produced by charged particles on the spectral lines is essential for spectroscopic diagnostic and atomic structure calculations. Therefore, accurate measurements of Stark broadening and shift parameters are required in laboratory plasma research, atomic structure calculations, and to analyse astrophysical data.

A large number of ionized vanadium spectral lines has been observed in stellar objects and solar plasma, being overabundant in some A-type stars (van't Veer-Mennert et al. 1985; Sadakane et al. 1989), where the Stark broadening is the main pressure broadening mechanism. In addition, some of these lines have been studied for the diagnostic of fusion plasmas because vanadium alloys are used in blanket applications.

Despite the interest of these applications, there are no accurate V II Stark width and shifts measurements and very few theoretical calculations. In 1983 and 1985, Lakićević made an estimation of the Stark broadening of some V II spectral lines only based on regularities and systematic trends. Until 2000 there have not been more sophisticated calculations, when Popović & Dimitrijević performed Stark broadening calculations for 14 transitions of VII. However, authors report that accuracy might be improved if reliable atomic data were available to perform the semiclassical method. Recently, Wood et al. (2014) have reported new experimental transition probability values for V II transitions, highlighting the need to measure simultaneously strong and very week lines in laboratory to explain unexpected trends in stellar abundance determinations. Also, Saloman & Kramida (2017) have critically evaluated atomic data for singly ionized vanadium.

The aim of this work is to provide for the first time experimental Stark width and shifts of V II lines. Our group has measured these parameters by using laser-induced breakdown spectroscopy (see for example Aguilera et al. 2014 and Manrique et al. 2019), developing a methodology that allows to perform simultaneously measurements for strong and weak spectral lines that are free of self-absorption through the selection of the suitable concentration of the studied element in the sample. In this work, we have studied Stark widths and shifts in the 2000–4200 Å wavelength range for strong and weak V II lines, including resonance and forbidden lines from 147 lines and 75 multiplets.

2 EXPERIMENT

A Q-switched Nd: YAG laser (wavelength 1064 nm, pulse width 4.5 ns, pulse energy 60 mJ) is used to generate the plasmas in air at atmospheric pressure. The focusing lens (focal length 126 mm) is placed at 122 mm from the sample surface. A pair of flat and concave (focal length 125 mm) mirrors is used to form a 1:1 image of the plasma on to the entrance of a Czerny–Turner spectrometer (focal length 0.75 m, grating of 3600 lines mm−1, slit width 20 μm). Using an ICCD (1200 × 256 effective pixels), the system provides a spectral resolution of 15 pm at 3000 Å. The sample is rotated at 100 rpm during spectra measurements, which accumulate the emission from 100 laser shots. To reduce the statistical error, we repeated each measurement at five different sample locations, averaging the resulting line width values.

★ E-mail: j.a.aguilera@unavarra.es

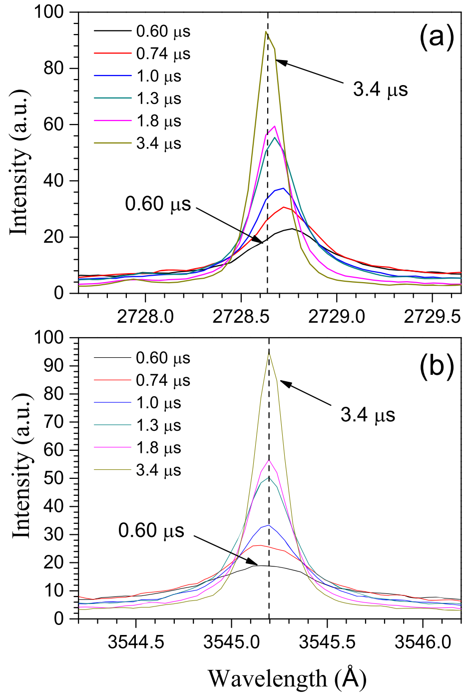

Figure 1. Spectra of the V II lines at 2728.637 Å (a) and 3545.196 Å (b), measured at different time windows centred at the indicated times.

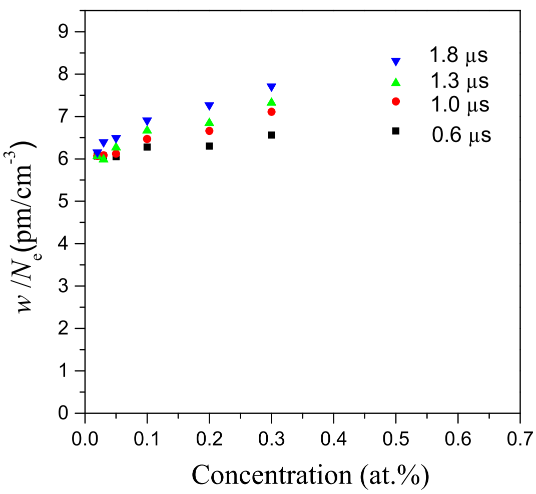

Figure 2. Ratio of the line width to the electron density against vanadium concentration for the V II line at 3102.300 Å measured at different time windows centred at the indicated times.

To avoid self-absorption, we select the atomic concentration of vanadium in the sample. By borate fusion of pure V_2O_5 in powder form, a set of seven samples were prepared as fused glass discs with increasing vanadium concentration from 0.02 to 0.5 at. per cent. To determine the electron density from the Stark-broadened profile of a Ca II line, a trace amount of CaO was also added to each sample, leading to 0.008 at. per cent calcium concentration.

3 RESULTS AND DISCUSSION

For each line of interest, we measured spectra with time delays from the laser pulse ranging from 0.57 to 3.1 μs, whilst time widths varied correspondingly from 0.06 to 0.6 μs. Therefore, the resulting six time windows were centred at instants 0.60, 0.74, 1.0, 1.3, 1.8, and 3.4 μs. An additional spectrum with 7 μs delay is used as a reference to obtain the Stark shifts, as the electron density has decreased to a negligible value at this late time of the plasma evolution. Fig. 1 shows the temporal decrease of the widths for two spectral lines resulting from the drop of the plasma electron density. As can be seen, the line width is higher for the line at 3545.196 Å (Fig. 1b) whereas the line shift is high and positive for the line at 2728.637 Å (Fig. 1a) and smaller in absolute value and negative for the 3545.196 Å line (Fig. 1b).

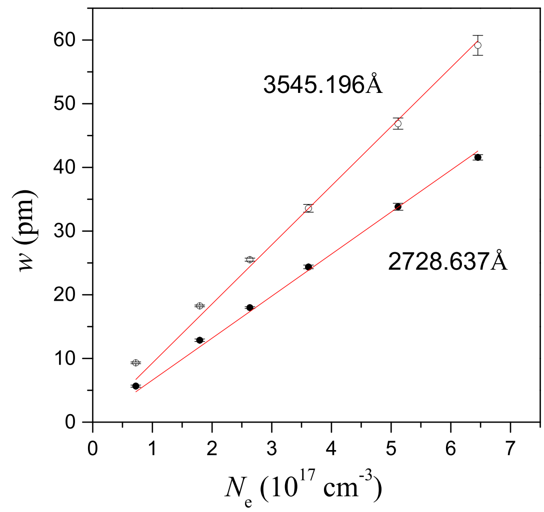

Figure 3. Line width as a function of the electron density for two V II lines. The error bars represent the standard deviation of the average for five repeated measurements. The final Stark widths are obtained as the slopes of the linear fittings with zero intercept.

In previous works (Manrique et al. 2019), the electron density was determined from the Stark broadening of the H α line, assuming that the measured value is valid for the whole set of samples. However, matrix effects could lead to a non-negligible variation of the electron density among the plasmas generated with the different samples. In this work, to be sure that the reference electron density and the profile of the line of interest are measured under the same conditions, we have determined the electron density in each measurement from the Stark width of the Ca II doublet at 3933.663 and 3968.469 Å. For the small calcium content in the samples (0.008 at. per cent), self-absorption of these lines is negligible. Moreover, for this low calcium concentration, the V II spectrum does not show overlapping with the Ca II spectrum. The electron density values deduced from the two Ca II lines are the same within the experimental error. For the Stark widths of these lines, we have used the experimental values reported by our group in a recent work (Aguilera et al. 2014) and checked again that the resulting electron densities are consistent with those determined using the H α line. The Lorentzian widths are obtained by fitting the experimental spectra to Voigt profiles with a fixed Gaussian component that includes the instrumental and Doppler profiles. The resulting electron density decreases from 6.5×10^{17} cm^{-3} at 0.6 μs to 0.72×10^{17} cm^{-3} at 3.4 μs. The plasma temperature at the different time windows is obtained from Boltzmann plots constructed using 22 V II lines with upper level energies in the range 4.29–6.88 eV and well-known transition probabilities (Kramida et al. 2019). The resulting temperature decreases from (14 900 $\pm$ 400) to (11 000 $\pm$ 100) K.

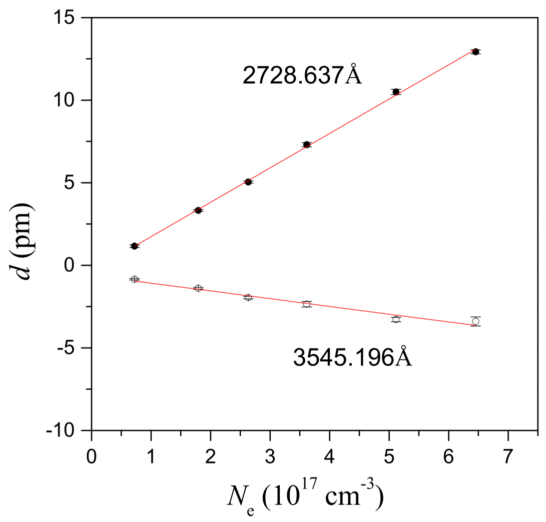

Figure 4. Line shift versus electron density for two V II lines. The error bars represent the standard deviation of the average for five repeated measurements. The Stark shifts are determined as the slopes of the linear plots with zero intercept.

To reduce the systematic error due to self-absorption, we have used the method based on CSigma graphs developed in recent years by our group (Aragón & Aguilera 2014). Starting from a set of characteristic plasma parameters obtained in previous experiments performed in the same conditions, this method allows us to estimate the vanadium concentration required to limit self-absorption to a maximum value fixed at 10 per cent. In this way, the V II lines are classified in seven groups according to their intensity and, for each group, a sample with the required concentration is prepared and used for the Stark width measurements. Even though we have checked in many experiments that this procedure is reliable to control self-absorption, we have performed an additional test for the lines of higher intensity, consisting in the measurement of the line width for the whole set of samples prepared with different concentrations. Fig. 2 shows the ratio of the line width to the electron density as a function of the concentration in the sample for the most intense line among those investigated (3102.300 Å) measured at different time windows. As expected, the line width increases with concentration due to self-absorption. The effect is more pronounced at late-time windows at which the drop of the electron density leads to a decrease of the Lorentzian width, which results in stronger self-absorption. As can be seen, the data for different concentrations and time windows converge to the same w/N_e value at the 0.02 at. per cent concentration. This is an indication that, by using this small concentration, the effect of self-absorption has been reduced to a value lower than about 10 per cent for this intense line.

Fig. 3 shows the experimental results for the line width as a function of the electron density for the lines at 2728.637 and 3545.196 Å, obtained from the spectra of Fig. 1. The corresponding plots for the line shift are shown in Fig. 4. In both cases the data show a linear dependence with the electron density, and the final values of the Stark width and shift is obtained from the slopes of the linear fittings. Therefore, the weak dependence on temperature of the Stark width has not been observed for the temperature range in our plasmas taking into account our experimental errors.

Our results for the Stark widths and shifts of the V II lines are listed in Table 1, compared with previous results from the literature. To facilitate the location of the data for a given line we include Table 2, which collects the lines ordered by wavelength, showing the multiplet number for each line and it is added in ASCII code as online supporting information. The total experimental error is estimated as 15 per cent and 11 per cent for the Stark widths and shifts, respectively. It arises from the quadratic combination of the uncertainty due to the plasma inhomogeneity (3 per cent), the electron density measurement (11 per cent), and the self-absorption of the plasma (10 per cent only for width measurements). Nevertheless, for the shift measurements, the minimum shift detectable with our wavelength resolution leads to a minimum absolute error of 0.1 pm.

The comparison of our results with the data obtained by Popović & Dimitrijević (2000) shows good agreement for width measurements, which are 8 per cent higher for the resonance lines than ours and around 30 per cent higher for 4p–4s transitions. The disagreement increases to 60 per cent for 4d–4p transitions with lower values. Comparison with the same reference for shift measurements shows only good agreement, approximately 10 per cent, for 4d–4p transitions. Nevertheless, values for the resonance lines are lower by a factor 8 than ours whilst for the rest of the transitions are higher by a factor between 4 and 10, depending on the transition. It is worth noticing that shift calculations have lower accuracy than width values and that the authors of these calculations explained that, due to the lack of reliable atomic data, simpler methods for the calculations had to be applied. Width and shift Stark earlier estimations reported by Lakićević (1983 and 1985) using simple dependence on ionization potential, show good agreement (better than 30 per cent) to our width measurements whilst shift values have poor agreement.

CONCLUSIONS

We report measurements of Stark widths of V II spectral lines performed by laser-induced breakdown spectroscopy. Widths are provided for 147 lines, and shifts for 117 lines. Special care has been taken to avoid the systematic effect due to self-absorption, for which the CSigma graph methodology has been used to determine suitable vanadium concentrations in the samples. To our knowledge, these are the first experimental Stark width and shift data for VII, which are necessary for plasma diagnostics and for comparison with theoretical calculations.

Table 1. Stark widths and shifts (pm) of V II spectral lines at electron density 10^{17} cm^{-3}. Temperature ranged from 11 000 to 14 900 K. The estimated relative error is 15 and 11 per cent for width and shift, respectively, with a minimum absolute error for shifts of 0.1 pm.

No	Transition[a]	Multiplet[a]	λ(Å)[a]	w	d	w^b	d^b
1	$3d^4$–$3d^3(^4F)4p$	$a\,^5D$–$z\,^3D^o$	2702.177	6.8	1.80		
2		a^5D–z^5F^o	2700.927	6.4	2.33	7.00	0.257
			2706.156	6.2	2.11	7.00	0.257
			2715.655	6.5	2.04	7.00	0.257
			2728.637	6.6	2.09	7.00	0.257
3		a^5D-z^5D^o	2687.952	6.4	2.08	6.81	– 0.0792
			2679.316	6.5	1.80	6.81	– 0.0792
			2672.000	6.4	1.93	6.81	– 0.0792
			2677.796	6.4	1.90	6.81	– 0.0792
4	$3d^4$–$3d^3(^4P)4p$	a^5D–y^5D^o	2131.835	3.8			
5	$3d^3(^4F)4\,s$–$3d^3(^4F)4p$	a^5F–z^5G^o	3102.300	6.1	– 0.19	9.14	– 2.14
			3110.710	6.0	– 0.26	9.14	– 2.14
			3118.382	6.4	– 0.32	9.14	– 2.14
			3125.286	7.0	– 0.42	9.14	– 2.14
			3126.219	6.0	– 0.26	9.14	– 2.14
			3130.270	6.0	– 0.33	9.14	– 2.14
			3133.334	6.3	– 0.25	9.14	– 2.14
6		a^5F–z^3D^o	2906.458	6.9	– 0.44		
			2957.521	5.6	– 0.48		
			2896.206	6.1	– 0.54		
			2903.075	6.2	– 0.40		
7		a^5F–z^5F^o	2944.571	5.6	– 0.20	8.89	– 1.36
			2952.071	6.1	– 0.46	8.89	– 1.36
			2911.063	6.2		8.89	– 1.36
			2934.401	5.9	– 0.50	8.89	– 1.36
			2930.808	5.4	– 0.19	8.89	– 1.36
8		a^5F–z^5D^o	2880.028	5.6	– 0.46	8.63	– 1.72
			2882.499	6.0	– 0.35	8.63	– 1.72
			2889.619	6.6		8.63	– 1.72
9		a^3F–z^3D^o	3556.800	8.6	– 0.46	12.6	– 2.84
			3545.196	8.3	– 0.54	12.6	– 2.84
			3589.759	9.1	– 0.65	12.6	– 2.84
			3520.019	8.6	– 0.43	12.6	– 2.84
10		a^3F–z^5F^o	3593.333	8.1	– 0.31		
			3592.022	8.9	– 0.49		
			3530.772	8.5	– 0.40		
			3560.590	7.7			
			3566.176	8.5	– 0.60		
11		a^3F–z^5D^o	3517.300	8.7	– 0.43		
			3504.436	7.9	– 0.53		
			3493.163	8.3			
			3485.921	8.7	– 0.79		
12		a^3F–z^3G^o	3276.125	7.7	– 0.31	11.6	– 2.51
			3271.122	8.0	– 0.39	11.6	– 2.51
			3267.702	8.0	– 0.37	11.6	– 2.51
			3298.738	7.5	– 0.24	11.6	– 2.51
13		a^3F–z^3F^o	3190.682	8.6	– 0.23	11.1	– 2.32
			3188.513	8.8	– 0.58	11.1	– 2.32
			3187.712	8.5		11.1	– 2.32
			3214.746	9.3		11.1	– 2.32
			3208.346	8.4		11.1	– 2.32
			3164.839	7.8		11.1	– 2.32
14	$3d^3(^4F)4\,s$–$3d^3(^2\,G)4p$	a^3F–y^3G^o	2514.637	5.6			
15	$3d^3(^4F)4\,s$–$3d^3(^2P)4p$	a^3F–y^3D^o	2380.913	4.3			
16	$3d^4$–$3d^3(^4F)4p$	a^3P2–z^3D^o	3951.956	12.6	3.5		
17		a^3P2–z^5F^o	3973.629	12.8	3.4		
18		a^3P2–z^5D^o	3903.252	11.6	3.5		
19	$3d^4$–$3d^3(^2P)4p$	a^3P2–y^3P^o	2549.277	5.5	1.31		
20	$3d^4$–$3d^3(^4F)4p$	a^3H–z^3G^o	3715.464	11.2	3.2		
			3732.747	12.6	3.3		
			3745.799	11.9	3.1		
21	$3d^4$–$3d^3(^2\,G)4p$	a^3H–y^3G^o	2765.663	9.2	2.5		
			2768.555	9.2	1.68		

Table 1 – *continued*

No	Transition^a	Multiplet^a	λ(Å)^a	*w*	*d*	w^b	d^b
22	$3d^4$–$3d^3(^2H)4p$	a^3H–x^3G^o	2352.178	4.7	1.73		
			2342.141	5.0	1.44		
23	$3d^4$–$3d^3(^4F)4p$	b^3F2–z^3F^o	3727.341	12.7	3.0		
			3770.966	12.5	3.3		
24	$3d^4$–$3d^3(^2G)4p$	b^3F2–y^3G^o	2836.516	7.2	1.99		
25		b^3F2–y^3F^o	2803.462	6.5	1.83		
			2802.792	7.9	1.81		
26	$3d^4$–$3d^3(^2D2)4p$	b^3F2–x^3F^o	2577.676	7.7	1.66		
27	$3d^3(^4P)4s$–$3d^3(^4P)4p$	a^5P–y^5D^o	2968.378	6.0			
			2983.562	6.2			
			3013.104	7.2	– 0.32		
			3022.580	6.8	– 0.52		
28	$3d^3(^4P)4s$–$3d^3(^4P)4p$	a^5P–z^5P^o	3001.204	5.8	– 0.26		
			3014.821	6.0	– 0.25		
			2988.025	6.2	– 0.32		
			2995.999	6.3	– 0.39		
29	$3d^4$–$3d^3(^4F)4p$	a^3G–z^3G^o	4005.702	12.1	1.96		
			4023.378	13.0	2.41		
			4035.620	13.6	2.42		
30		a^3G–z^3F^o	3878.707	13.0	2.30		
			3899.128	13.2	2.27		
			3914.321	13.5	2.07		
31	$3d^4$–$3d^3(^2G)4p$	a^3G–z^3H^o	3067.104	6.6	1.15		
32		a^3G–y^3F^o	2888.240	7.5	1.11		
33	$3d^4$–$3d^3(^2D2)4p$	a^3G–x^3F^o	2630.664	6.3	1.08		
			2642.206	6.7			
			2645.836	6.0	1.25		
34	$3d^4$–$3d^3(^2H)4p$	a^3G–x^3G^o	2465.270	5.2	1.04		
			2453.346	4.7	1.05		
35	$3d^3(^2G)4s$–$3d^3(^4F)4p$	b^3G–z^3F^o	4183.429	13.0	1.32		
36	$3d^3(^2G)4s$–$3d^3(^2G)4p$	b^3G–z^3H^o	3217.109	7.1	0.90		
			3237.870	8.6	1.01		
			3254.765	7.6	0.79		
37	$3d^3(^2G)4s$–$3d^3(^2G)4p$	b^3G–y^3G^o	3100.932	8.5	1.16		
38		b^3G–y^3F^o	3041.416	8.1	0.88		
			3042.261	7.8	0.95		
39		b^3G–z^1H^o	3023.884	7.3	0.85		
40		b^3G–z^1G^o	3012.016	7.8	0.93		
41	$3d^3(^2G)4s$–$3d^3(^2H)4p$	b^3G–y^3H^o	2797.012	7.1	0.73		
42	$3d^3(^2G)4s$–$3d^3(^2H)4p$	b^3G–x^3G^o	2584.951	5.7	0.89		
43	$3d^4$–$3d^3(^2G)4p$	a^1G2–z^1H^o	3155.404	9.0	1.73		
44		a^1G2–z^1G^o	3142.482	7.8	1.19		
45	$3d^4$–$3d^3(^2D2)4p$	a^3D–w^3D^o	2819.431	6.1	1.23		
			2817.495	6.4	1.25		
46	$3d^3(^2G)4s$–$3d^3(^2G)4p$	b^1G–z^1F^o	3282.529	7.9	0.34		
47		b^1G–z^1G^o	3265.886	9.4			
48	$3d^3(^2P)4s$–$3d^3(^4P)4p$	b^3P–z^3P^o	3621.208	11.5			
49	$3d^3(^2P)4s$–$3d^3(^2P)4p$	b^3P–z^3S^o	3024.983	6.6			
			3028.054	6.9			
50	$3d^3(^2P)4s$–$3d^3(^2P)4p$	b^3P–x^3F^o	3005.813	6.9			
51		b^3P–x^3D^o	2972.263	7.2			
			2981.200	6.8			
52	$3d^4$–$3d^3(^2H)4p$	a^1I–x^3G^o	2775.760	7.1	2.6		
53	$3d^3(^4P)4s$–$3d^3(^4P)4p$	c^3P–z^3P^o	3787.239	10.5	0.35		
54	3d3(4P)4 s–3d3(2P)4p	c3P–y3Do	3251.864	8.6	0.60		
			3257.886	8.4	0.20		
55	$3d^3(^4P)4s$–$3d^3(^4P)4p$	c^3P–x^3D^o	3083.209	8.6			
56	$3d^3(^2H)4s$–$3d^3(^2G)4p$	b^3H–z^3H^o	3669.423	9.3	– 0.27		
57	$3d^3(^2H)4s$–$3d^3(^2H)4p$	b^3H–y^3H^o	3136.517	7.1	– 0.35		
			3139.745	7.1	– 0.31		
58		b^3H–z^3I^o	3063.244	6.7			
59		b^3H–x^3G^o	2869.132	6.3			
			2854.335	6.5			
			2847.572	6.4			
60		b^3H–y^1H^o	2845.244	8.4			

Table 1 – *continued*

No	Transition[a]	Multiplet[a]	λ(Å)[a]	w	d	w[b]	d[b]
61	$3d^3(^2H)4\,s$–$3d^2(^3F)4s4p(^3P*)$	b^3H–v^3G^o	2023.565	3.1			
62	$3d^3(^2D2)4\,s$–$3d^3(^2D2)4p$	b^3D–x^3F^o	3151.316	7.7	1.33		
63	$3d^4$–$3d^3(^2\,G)4p$	a^1D2–z^1F^o	3497.027	10.1	1.58		
64	$3d^3(^2P)4\,s$–$3d^3(^2P)4p$	a^1P–$z\,^1S^o$	3847.334	10.1	– 1.40		
65		a^1P–z^1D^o	3618.927	10.2	– 1.17		
66		a^1P–y^1P^o	2949.176	6.3			
67	$3d^3(^2H)4\,s$–$3d^3(^2H)4p$	a^1H–y^1G^o	3250.773	7.9	– 0.65		
68		a^1H–y^1H^o	3113.564	7.9	– 0.35		
69	$3d^3(^2D2)4\,s$–$3d^3(^2D2)4p$	b^1D–y^1F^o	3337.823	9.7	1.98		
70	$3d^4$ –$3d^3(^2H)4p$	a^1F–y^1G^o	3661.365	11.1	2.9		
71	$3d^3(^2F)4\,s$–$3d^3(^2F)4p$	c^3F–w^3G^o	2955.579	7.7	1.43		
72	$3d^4$–$3d^3(^2F)4p$	d^3F1–w^3F^o	3174.533	7.5			
73		d^3F1–w^3G^o	2973.971	6.9	1.29		
			2985.179	6.9	0.71		
74	$3d^3(^4F)4p$–$3d^3(^4F)4d$	z^5G^o–e^5H	2663.208	16.3	7.8	11.3	8.11
			2655.647	18.1	8.4	11.3	8.11
			2649.325	19.4	8.2	11.3	8.11
			2644.332	20.5	7.1	11.3	8.11
75		z^3G^o–e^3H	2781.399	22.5	11.6	14.7	9.87

[a]Data from Kramida et al. 2019.
[b]Popović & Dimitrijević (2000). Data reported for a temperature of 10 000 K.

ACKNOWLEDGEMENTS

This work has been supported by the project PGC2018-0942096-B-I00 of the Spanish Ministerio de Ciencia, Innovación y Universidades. DDP acknowledges the support of Consejo Nacional de Investigaciones Científicas y Técnicas (CONICET) of Argentina.

DATA AVAILABILITY

The data underlying this article are available in the article and in its online supplementary material.

REFERENCES

Aguilera J. A., Aragón C., Manrique J., 2014, MNRAS, 444, 1854
Aragón C., Aguilera J. A., 2014, JQSRT, 149, 90
Kramida A., , Ralchenko Yu., Reader J., and NIST ASD Team, 2019, NIST Atomic Spectra Database (ver. 5.7.1). National Institute of Standards and Technology, Gaithersburg, MD
Lakićević I. S., 1983, A&AS, 127, 37
Lakićević I. S., 1985, A&AS, 151, 457
Manrique J., Aragón C, Aguilera J. A., 2019, MNRAS, 482, 1931
Popović L. Č., Dimitrijević M. S., 2000, Phys. Scr., 61, 192
Sadakane K., Ueta M., 1989, Publ. Astron. Soc. Japan, 41, 279
Saloman E., Kramida A., 2017, ApJS, 231, 19
van't Veer-Mennert C., Coupry M. F., Bukhart C., 1985, A&AS, 146, 139
Wood M. P., Lawler J. E., Den Hartog E. A., Sneden C., Cowan J. J., 2014, ApJS, 214, 18

SUPPORTING INFORMATION

Supplementary data are available at *MNRAS* online.

Table S3. List of measured Stark widths and shifts, ordered by wavelength.

Please note: Oxford University Press is not responsible for the content or functionality of any supporting materials supplied by the authors. Any queries (other than missing material) should be directed to the corresponding author for the article.

This paper has been typeset from a Microsoft Word file prepared by the author.

Table 2. List of lines with reported Stark width or shift, ordered by wavelength and with multiplet number for faster location in Table 1.

λ (Å)	No
2023.565	61
2131.835	4
2342.141	22
2352.178	22
2380.913	15
2453.346	34
2465.270	34
2514.637	14
2549.277	19
2577.676	26
2584.951	42
2630.664	33
2642.206	33
2644.332	74
2645.836	33
2649.325	74
2655.647	74
2663.208	74
2672.000	3
2677.796	3
2679.316	3
2687.952	3
2700.927	2
2702.177	1
2706.156	2
2715.655	2
2728.637	2
2765.663	21
2768.555	21
2775.760	52
2781.399	75
2797.012	41
2802.792	25
2803.462	25
2817.495	45
2819.431	45
2836.516	24
2845.244	60
2847.572	59
2854.335	59
2869.132	59
2880.028	8
2882.499	8
2888.240	32
2889.619	8
2896.206	6
2903.075	6
2906.458	6
2911.063	7
2930.808	7
2934.401	7
2944.571	7
2949.176	66
2952.071	7
2955.579	71
2957.521	6
2968.378	27
2972.263	51
2973.971	73
2981.200	51
2983.562	27
2985.179	73
2988.025	28

Table 2 – *continued*

λ (Å)	No
2995.999	28
3001.204	28
3005.813	50
3012.016	40
3013.104	27
3014.821	28
3022.580	27
3023.884	39
3024.983	49
3028.054	49
3041.416	38
3042.261	38
3063.244	58
3067.104	31
3083.209	55
3100.932	37
3102.300	5
3110.710	5
3113.564	68
3118.382	5
3125.286	5
3126.219	5
3130.270	5
3133.334	5
3136.517	57
3139.745	57
3142.482	44
3151.316	62
3155.404	43
3164.839	13
3174.533	72
3187.712	13
3188.513	13
3190.682	13
3208.346	13
3214.746	13
3217.109	36
3237.870	36
3250.773	67
3251.864	54
3254.765	36
3257.886	54
3265.886	47
3267.702	12
3271.122	12
3276.125	12
3282.529	46
3298.738	12
3337.823	69
3485.921	11
3493.163	11
3497.027	63
3504.436	11
3517.300	11
3520.019	9
3530.772	10
3545.196	9
3556.800	9
3560.590	10
3566.176	10
3589.759	9
3592.022	10
3593.333	10
3618.927	65
3621.208	48

Table 2 – *continued*

λ (Å)	No
3661.365	70
3669.423	56
3715.464	20
3727.341	23
3732.747	20
3745.799	20
3770.966	23
3787.239	53
3847.334	64
3878.707	30
3899.128	30
3903.252	18
3914.321	30
3951.956	16
3973.629	17
4005.702	29
4023.378	29
4035.620	29
4183.429	35

List of astronomical key words (Updated on 2020 January)

This list is common to *Monthly Notices of the Royal Astronomical Society, Astronomy and Astrophysics*, and *The Astrophysical Journal*. In order to ease the search, the key words are subdivided into broad categories. No more than *six* subcategories altogether should be listed for a paper.

The subcategories in boldface containing the word 'individual' are intended for use with specific astronomical objects; these should never be used alone, but always in combination with the most common names for the astronomical objects in question. Note that each object counts as one subcategory within the allowed limit of six.

The parts of the key words in italics are for reference only and should be omitted when the keywords are entered on the manuscript.

General
editorials, notices
errata, addenda
extraterrestrial intelligence
history and philosophy of astronomy
miscellaneous
obituaries, biographies
publications, bibliography
sociology of astronomy
standards

Physical data and processes
acceleration of particles
accretion, accretion discs
asteroseismology
astrobiology
astrochemistry
astroparticle physics
atomic data
atomic processes
black hole physics
chaos
conduction
convection
dense matter
diffusion
dynamo
elementary particles
equation of state
gravitation
gravitational lensing: micro
gravitational lensing: strong
gravitational lensing: weak
gravitational waves
hydrodynamics
instabilities
line: formation
line: identification
line: profiles
magnetic fields
magnetic reconnection
(magnetohydrodynamics) MHD
masers
molecular data
molecular processes
neutrinos
nuclear reactions, nucleosynthesis, abundances
opacity
plasmas
polarization
radiation: dynamics
radiation mechanisms:general
radiation mechanisms: non-thermal
radiation mechanisms: thermal
radiative transfer
relativistic processes
scattering
shock waves
solid state: refractory
solid state: volatile
turbulence
waves

Astronomical instrumentation, methods and techniques
atmospheric effects
balloons
instrumentation: adaptive optics
instrumentation: detectors
instrumentation: high angular resolution
instrumentation: interferometers
instrumentation: miscellaneous
instrumentation: photometers
instrumentation: polarimeters
instrumentation: spectrographs
light pollution
methods: analytical
methods: data analysis
methods: laboratory: atomic
methods: laboratory: molecular
methods: laboratory: solid state
methods: miscellaneous
methods: numerical
methods: observational
methods: statistical
site testing
space vehicles
space vehicles: instruments
techniques: high angular resolution
techniques: image processing
techniques: imaging spectroscopy
techniques: interferometric
techniques: miscellaneous
techniques: photometric
techniques: polarimetric
techniques: radar astronomy
techniques: radial velocities
techniques: spectroscopic
telescopes

Astronomical data bases
astronomical data bases: miscellaneous
atlases
catalogues
surveys
virtual observatory tools

Software
software: data analysis
software: development
software: documentation
software: public release
software: simulations

Astrometry and celestial mechanics
astrometry
celestial mechanics
eclipses
ephemerides
occultations
parallaxes
proper motions
reference systems
time

The Sun
Sun: abundances
Sun: activity
Sun: atmosphere
Sun: chromosphere
Sun: corona
Sun: coronal mass ejections (CMEs)
Sun: evolution
Sun: faculae, plages
Sun: filaments, prominences
Sun: flares
Sun: fundamental parameters
Sun: general
Sun: granulation
Sun: helioseismology
Sun: heliosphere
Sun: infrared
Sun: interior
Sun: magnetic fields
Sun: oscillations
Sun: particle emission
Sun: photosphere
Sun: radio radiation
Sun: rotation
(Sun:) solar–terrestrial relations
(Sun:) solar wind
(Sun:) sunspots
Sun: transition region
Sun: UV radiation
Sun: X-rays, gamma-rays

Planetary systems
comets: general

comets: individual: . . .
Earth
interplanetary medium
Kuiper belt: general

Kuiper belt objects: individual: . . .
meteorites, meteors, meteoroids
minor planets, asteroids: general
minor planets, asteroids: individual: . . .
Moon
Oort Cloud
planets and satellites: atmospheres
planets and satellites: aurorae
planets and satellites: composition
planets and satellites: detection
planets and satellites: dynamical evolution and stability
planets and satellites: formation
planets and satellites: fundamental parameters
planets and satellites: gaseous planets
planets and satellites: general

planets and satellites: individual: . . .
planets and satellites: interiors
planets and satellites: magnetic fields
planets and satellites: oceans
planets and satellites: physical evolution
planets and satellites: rings
planets and satellites: surfaces
planets and satellites: tectonics
planets and satellites: terrestrial planets
planet–disc interactions
planet–star interactions
protoplanetary discs
zodiacal dust

Stars
stars: abundances
stars: activity
stars: AGB and post-AGB
stars: atmospheres
(stars:) binaries *(including multiple)*: close
(stars:) binaries: eclipsing
(stars:) binaries: general
(stars:) binaries: spectroscopic
(stars:) binaries: symbiotic
(stars:) binaries: visual
stars: black holes
(stars:) blue stragglers
(stars:) brown dwarfs
stars: carbon
stars: chemically peculiar
stars: chromospheres
(stars:) circumstellar matter
stars: coronae
stars: distances
stars: dwarf novae
stars: early-type
stars: emission-line, Be
stars: evolution
stars: flare
stars: formation
stars: fundamental parameters
(stars:) gamma-ray burst: general
(stars:) **gamma-ray burst: individual: . . .**
stars: general
(stars:) Hertzsprung–Russell and colour–magnitude diagrams
stars: horizontal branch
stars: imaging
stars: individual: . . .
stars: interiors

stars: jets
stars: kinematics and dynamics
stars: late-type
stars: low-mass
stars: luminosity function, mass function
stars: magnetars
stars: magnetic field
stars: massive
stars: mass-loss
stars: neutron
(stars:) novae, cataclysmic variables
stars: oscillations *(including pulsations)*
stars: peculiar *(except chemically peculiar)*
(stars:) planetary systems
stars: Population II
stars: Population III
stars: pre-main-sequence
stars: protostars
(stars:) pulsars: general
(stars:) **pulsars: individual: . . .**
stars: rotation
stars: solar-type
(stars:) starspots
stars: statistics
(stars:) subdwarfs
(stars:) supergiants
(stars:) supernovae: general
(stars:) **supernovae: individual: . . .**
stars: variables: Cepheids
stars: variables: Scuti
stars: variables: general
stars: variables: RR Lyrae
stars: variables: S Doradus
stars: variables: T Tauri, Herbig Ae/Be
(stars:) white dwarfs
stars: winds, outflows
stars: Wolf–Rayet

Interstellar medium (ISM), nebulae
ISM: abundances
ISM: atoms
ISM: bubbles
ISM: clouds
(ISM:) cosmic rays
(ISM:) dust, extinction
ISM: evolution
ISM: general
(ISM:) HII regions
(ISM:) Herbig–Haro objects

ISM: individual objects: . . .
(except planetary nebulae)
ISM: jets and outflows
ISM: kinematics and dynamics
ISM: lines and bands
ISM: magnetic fields
ISM: molecules
(ISM:) photodissociation region (PDR)
(ISM:) planetary nebulae: general
(ISM:) **planetary nebulae: individual: . . .**
ISM: structure
ISM: supernova remnants

The Galaxy
Galaxy: abundances
Galaxy: bulge
Galaxy: centre
Galaxy: disc
Galaxy: evolution
Galaxy: formation
Galaxy: fundamental parameters
Galaxy: general
(Galaxy:) globular clusters: general
(Galaxy:) **globular clusters: individual: . . .**
Galaxy: halo
Galaxy: kinematics and dynamics
(Galaxy:) local interstellar matter
Galaxy: nucleus
(Galaxy:) open clusters and associations: general
(Galaxy:) **open clusters and associations: individual: . . .**
(Galaxy:) solar neighbourhood
Galaxy: stellar content
Galaxy: structure

Galaxies
galaxies: abundances
galaxies: active
galaxies: bar
(galaxies:) BL Lacertae objects: general
(galaxies:) **BL Lacertae objects: individual: . . .**
galaxies: bulges
galaxies: clusters: general

galaxies: clusters: individual: . . .
galaxies: clusters: intracluster medium
galaxies: disc
galaxies: distances and redshifts
galaxies: dwarf
galaxies: elliptical and lenticular, cD
galaxies: evolution
galaxies: formation
galaxies: fundamental parameters
galaxies: general
galaxies: groups: general

galaxies: groups: individual: . . .
galaxies: haloes
galaxies: high-redshift

galaxies: individual: . . .
galaxies: interactions
(galaxies:) intergalactic medium
galaxies: irregular
galaxies: ISM
galaxies: jets
galaxies: kinematics and dynamics
(galaxies:) Local Group
galaxies: luminosity function, mass function
(galaxies:) Magellanic Clouds
galaxies: magnetic fields
galaxies: nuclei
galaxies: peculiar
galaxies: photometry
(galaxies:) quasars: absorption lines
(galaxies:) quasars: emission lines
(galaxies:) quasars: general

(galaxies:) **quasars: individual: . . .**
(galaxies:) quasars: supermassive black holes
galaxies: Seyfert
galaxies: spiral
galaxies: starburst
galaxies: star clusters: general

galaxies: star clusters: individual: . . .
galaxies: star formation
galaxies: statistics
galaxies: stellar content
galaxies: structure

Cosmology
(cosmology:) cosmic background radiation
(cosmology:) cosmological parameters
(cosmology:) dark ages, reionization, first stars
(cosmology:) dark energy
(cosmology:) dark matter
(cosmology:) diffuse radiation
(cosmology:) distance scale
(cosmology:) early Universe
(cosmology:) inflation
(cosmology:) large-scale structure of Universe
cosmology: miscellaneous
cosmology: observations
(cosmology:) primordial nucleosynthesis
cosmology: theory

Resolved and unresolved sources as a function of wavelength
gamma-rays: diffuse background
gamma-rays: galaxies
gamma-rays: galaxies: clusters
gamma-rays: general
gamma-rays: ISM
gamma-rays: stars
infrared: diffuse background
infrared: galaxies
infrared: general
infrared: ISM
infrared: planetary systems
infrared: stars
radio continuum: galaxies
radio continuum: general
radio continuum: ISM
radio continuum: planetary systems
radio continuum: stars
radio continuum: transients
radio lines: galaxies
radio lines: general
radio lines: ISM
radio lines: planetary systems
radio lines: stars
submillimetre: diffuse background
submillimetre: galaxies
submillimetre: general
submillimetre: ISM
submillimetre: planetary systems
submillimetre: stars
ultraviolet: galaxies
ultraviolet: general
ultraviolet: ISM
ultraviolet: planetary systems
ultraviolet: stars
X-rays: binaries
X-rays: bursts
X-rays: diffuse background
X-rays: galaxies
X-rays: galaxies: clusters
X-rays: general
X-rays: individual: . . .
X-rays: ISM
X-rays: stars

Transients
(transients:) black hole mergers
(transients:) black hole - neutron star mergers
(transients:) fast radio bursts
(transients:) gamma-ray bursts
(transients:) neutron star mergers
transients: novae
transients: supernovae
transients: tidal disruption events